A molecular beam/surface spectroscopy apparatus for the study of reactions on complex model catalysts

J. Libuda,[a] I. Meusel, J. Hartmann, and H.-J. Freund
Fritz-Haber-Institut der Max-Planck-Gesellschaft, Faradayweg 4-6, 14195 Berlin, Germany

(Received 22 March 2000; accepted for publication 7 August 2000)

We describe a newly developed ultrahigh vacuum (UHV) experiment which combines molecular beam techniques and *in situ* surface spectroscopy. It has been specifically designed to study the reaction kinetics and dynamics on complex model catalysts. The UHV system contains: (a) a preparation compartment providing the experimental techniques which are required to prepare and characterize single-crystal based model catalysts such as ordered oxide surfaces or oxide supported metal particles; and (b) the actual scattering chamber, where up to three molecular beams can be crossed on the sample surface. Two beams are produced by newly developed differentially pumped sources based on multichannel arrays. The latter are capable of providing high intensity and purity beams and can be modulated by means of a vacuum-motor driven and computer-controlled chopper. The third beam is generated in a continuous or pulsed supersonic expansion and is modulated via a variable duty-cycle chopper. Angular and time-resolved measurements of desorbing and scattered molecules are performed with a rotatable doubly differentially pumped quadrupole mass spectrometer with a liquid-nitrogen cooled ionizer housing. Time-resolved but angle-integrated measurements are realized with a second nondifferentially pumped quadrupole mass spectrometer. *In situ* measurements of adsorbed species under reaction conditions are performed by means of an adapted vacuum Fourier transform infrared spectrometer. The spectrometer provides the possibility of time-resolved measurements and can be synchronized with any of the beam sources. This contribution provides a general overview of the system and a description of all new components and their interplay. We also present test data for all components employing simple adsorption/desorption and reaction systems. © *2000 American Institute of Physics.* [S0034-6748(00)04011-9]

I. INTRODUCTION

Molecular beam techniques have established themselves among the most powerful tools to provide information on the kinetics and dynamics of gas-surface reactions and have been successfully applied to several catalytic reactions on simple single-crystal surfaces (see e.g., Refs. 1–3 and references therein). In contrast to these simple model surfaces, real catalysts are in most cases characterized by a complex heterogeneous and nanostructured surface and, therefore, show kinetic effects which cannot be reproduced on perfect single-crystalline systems.[4,5] Unfortunately, their complexity, heterogeneity, and high surface area, being responsible for the specific catalytic activities, precludes studies using many standard surface science techniques. One strategy that has been pursued to overcome this problem, frequently denoted as the ''material gap'' between surface science and catalysis, is the recent development of a variety of model systems based on ordered oxide surfaces.[5–8] In contrast to simple metal single crystals these systems can model the properties of compound-based or supported catalysts but, unlike most real catalysts, they are still easily accessible to most surface-science experimental techniques and provide well defined surface properties. Several examples of this type of systems have been intensively characterized in our group[7,8] as well as by others[5,6] with respect to their geometric structure, electronic properties, and adsorption behavior.

In order to link this knowledge to catalytic activities, we have set up a new molecular beam experiment, which is specifically designed to study model catalysis on these systems and to extract information on the kinetics under most well-defined conditions. The specific requirements for such a experiment can be summarized as follows:

(1) *Sample preparation and characterization*. The preparation and characterization techniques to prepare the specific type of model system must be integrated. A sample transfer to other vacuum systems can provide experimental techniques, which cannot be integrated in the molecular beam system itself.

(2) *Beam sources*. The beam sources should allow the beam flux and modulation frequency to be varied over a large parameter range. Long-term stability and high beam purity are an important issue if large gas exposures are necessary. For complex experiments, which require exposure to several reactants, it is advisable to integrate more than one beam source in order to avoid exposure from the background pressure.

(3) *Gas phase detection*. The gas phase detection must include an integral measurement of sticking and reaction probabilities. Additionally, information on the reaction dynamics can be obtained via an angular resolved detection of

[a]Author to whom correspondence should be addressed; electronic mail: libuda@fhi-berlin.mpg.de

gas phase molecules.[2,9,10] For complex surfaces angular resolution may be particularly important as it may allow a separation between various adsorption/desorption or reaction channels.[5] Both integral and angular resolved detectors should also provide temporal resolution on the time scale of the reaction or scattering experiment (typically from the microsecond to the second range).

(4) *Surface species detection.* In particular for heterogeneous surfaces, where various different species and adsorption sites may be present, *in situ* detection of surface species is a key feature of the experiment. Here, the main requirements are chemical specificity, compatibility with rough and structured surfaces, and a low data-acquisition time which allows *in situ* time-resolved studies.

So far, several molecular beam experiments for the study of gas surface reactions have been described in the literature[1,3,9,11–23] and various reviews can be found on experimental techniques and the design of molecular beam systems and components.[2,3,9,10,24] The first group of experiments have been specifically built to study the dynamics of gas surface interactions.[3,9,11,19,21–23] Such experiments basically require one supersonic beam source with maximum control of its dynamic parameters and an optimized angular and time-resolved detection of the scattered beam. The corresponding experiments may require velocity measurements and/or state-specific laser spectroscopic detection of scattered/desorbing molecules. As we will mainly focus on surface kinetics, here we will not discuss these instruments further. The second class of beam systems which shall be mentioned were designed to elucidate the kinetics and mechanism of surface reactions but can also be used to address questions of reaction dynamics.[11,12,17,18,22,23] In most cases the gas-phase detector was chosen to be a quadrupole mass spectrometer (QMS) with minimized sample–ionizer distance for kinetic studies and larger distance for velocity measurements. Some of these instruments are equipped with two or three beam sources, for example those described by Sibener *et al.*[22,23,25] or Ceyer *et al.*[11] Only a few attempts have been made to incorporate *in situ* spectroscopy into the experiment. This is however crucial, not only for identification of the nature of surface chemical species but also for *in situ* coverage measurements, which are an essential issue in quantitative kinetic studies. Sibener *et al.* have pointed out that He reflectivity measurements are a natural and highly sensitive way of coverage measurement in a molecular beam relaxation spectroscopy experiment.[25] This is, however, not feasible in the case of complex heterogeneous or nanostructured systems, as the large surface corrugation will completely quench the He reflectivity. Other surface detection methods that have been used in connection with beam experiments are electron energy loss spectroscopy[14,26] and Auger electron spectroscopy.[26,27] Bowker *et al.* have described an apparatus, which combines an effusive source and Fourier transform-infrared (FT-IR) spectroscopy.[28] Although the combination of beam techniques and surface spectroscopy has proven to be very valuable, attempts to develop *in situ* spectroscopies with the intention of extracting kinetic data during a reaction are scarce, due to long data acquisition times or limited chemical specificity.

In this article we describe a molecular beam/surface spectroscopy apparatus, which for the first time combines all features mentioned above: The ultrahigh vacuum (UHV) system is divided into a sample preparation and characterization and the actual scattering chamber: Here, up to three molecular beams can be crossed on the sample surface. Two beams are generated by newly developed differentially pumped and computer controlled multichannel array based sources. Together with a third chopped beam generated in a continuous or pulsed supersonic expansion, flexible flux modulation schemes can be provided. Angular and time-resolved gas phase detection is realized by means of a rotatable doubly differentially pumped QMS with liquid-nitrogen cooled ionizer housing and can be combined with angle integrated measurements by a second nondifferentially pumped QMS. *In situ* measurements of adsorbed species under reaction conditions are performed by means of an adapted vacuum FT-IR spectrometer. The high sensitivity and long-term stability of the spectrometer allows *in situ* measurements with short data acquisition times and—in combination with accumulation techniques—time-resolved measurements on the time scale of the beam experiment.

In Sec. II we will first provide a general overview over the apparatus and describe the interplay between the components followed by a more detailed description of the newly developed components and technical details. In Sec. III we will present first test data of all components employing simple adsorption/desorption and reaction systems.

II. SYSTEM DESIGN

A. General design considerations and overview

A schematic representation of the experimental arrangement is shown in Fig. 1. In order to avoid experiments involving background gas exposure even for more complex reaction or modulation schemes we have decided to equip the system with three beam sources: The first beam is generated in a supersonic expansion, providing a narrow velocity distribution. Modulated by a mechanical chopper which is operating at medium to high chopping frequencies it can be utilized to study the reaction kinetics and gas-surface dynamics (Fig. 1, molecular beam 1). We have decided to implement the beam sources 2 and 3 as multichannel-array based effusive sources, as they allow—due to reduced pumping requirements—a more compact design at higher beam intensities and an easy variation of the beam intensity over several orders of magnitude.[29] Complementary to the supersonic beam, the effusive sources are designed for surface kinetic studies at low modulation frequencies and variable intensity and allow large coverage modulation amplitudes. The scattering plane for dynamic studies is determined by the detection plane of the angular resolved detector so that the supersonic source is located in the same plane. As the effusive beams are used for surface coverage modulation in kinetic studies only, their direction is less critical and they are positioned out of plane. The exact incidence angles are given in Table I.

For the angular resolved detection of gas phase species several techniques have been applied such as photoioniza-

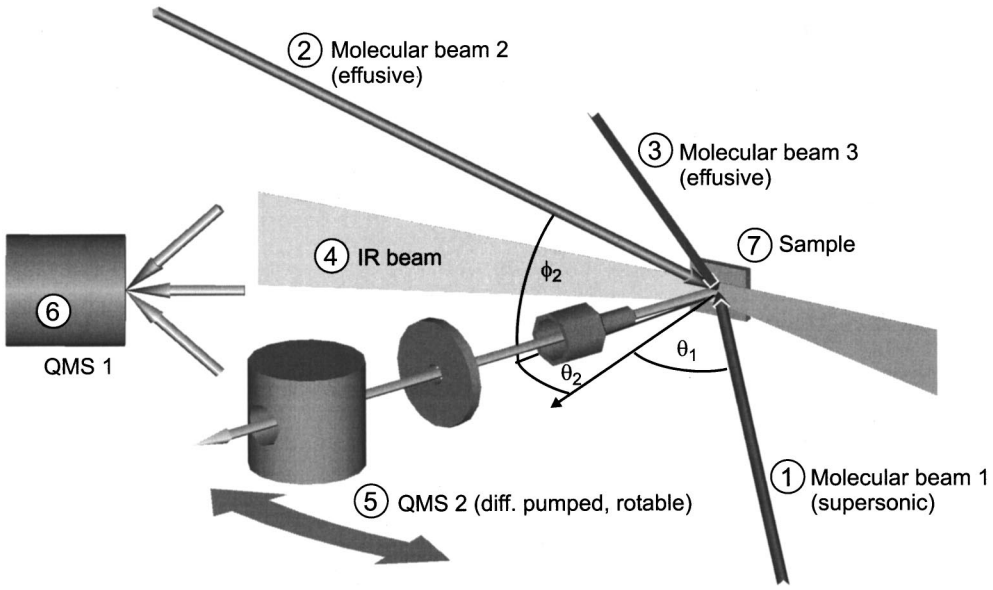

FIG. 1. Schematic representation of the experiment. The exact beam detector geometry are given in Table I.

tion, bolometric detection, or mass spectroscopy.[24] As a bolometric detection cannot provide chemical specificity, the latter is the most straightforward detection method, if we do not focus on the additional spectroscopic potential of multiphoton ionization. However, a QMS detection will result in an intrinsically lower sensitivity compared to the before mentioned methods. Therefore, it is helpful to reduce the signal-to-noise ratio by differential pumping of the detector region. We have integrated two differential pumping stages. Additionally, the inner pumping stage can be cooled by liquid nitrogen to further reduce the background pressure of condensable gases.

For the measurements of global reaction rates and sticking coefficients, a nondifferentially pumped QMS is required. The nondifferential pumped QMS is positioned in the scattering plane in order to keep the possibility of future time of flight (TOF) measurements (additional differential pumping would be necessary). However, as for angular integrated measurements the detector should not be in direct line of sight of the sample, the angular resolved detector can be positioned in between the QMS and sample.

In situ studies of adsorbed species require the potential to separate between similar adsorbed species and different adsorption sites. Among the various vibrational spectroscopies that meet these requirements, FT-IR spectroscopy provides the lowest data acquisition times and highest spectral resolution. Additionally, the grazing reflection geometry for infrared reflection absorption spectroscopy (IRAS) on metal surfaces simplifies the arrangement of the various components.

Finally, the preparation of complex samples requires several preparation methods. Due to the spatial restraints in the scattering chamber, we have separated the system into a preparation chamber and a scattering chamber. Both parts are set up as independent UHV systems separated by a gate valve. They are capable of reaching and maintaining a base pressure of 1×10^{-10} mbar. The sample is mounted on a long travel manipulator (VG Omniax), which allows transfer between both chambers. A general overview over the apparatus is given in Fig. 2.

The apparatus is mounted on a frame based on a standard framework system (Rose+Krieger), which for clarity is not shown in the figure. The experimentalist can reach all components from a two level operating platform that is decoupled from the support frame.

B. Sample preparation chamber

The preparation chamber is pumped by a combination of a turbomolecular pump (TMP) (Pfeiffer TMU400MC) and a Ti sublimation pump, which is only operated after preparation procedures involving large gas exposures. For preparation a differentially pumped ion gun (Omicron, ISE 10) and a low energy electron diffraction (LEED)/Auger system

TABLE I. Beam and detector geometries (see Fig. 1).

Component	Incidence and detection angles θ	ϕ	
Beam source 1 (supersonic)	−35°	0°	
Beam source 2 (effusive)	−25°	+35°	total incidence angle: 42.1°
Beam source 3 (effusive)	+20°	+35°	total incidence angle: 39.7°
QMS 1	−10°	0°	
QMS 2 (rotatable)	−180° to +180°	0°	detection angles using beam source 1: −180° to −70°; −5° to +180°
FTIR	+83°/−83°	0°	

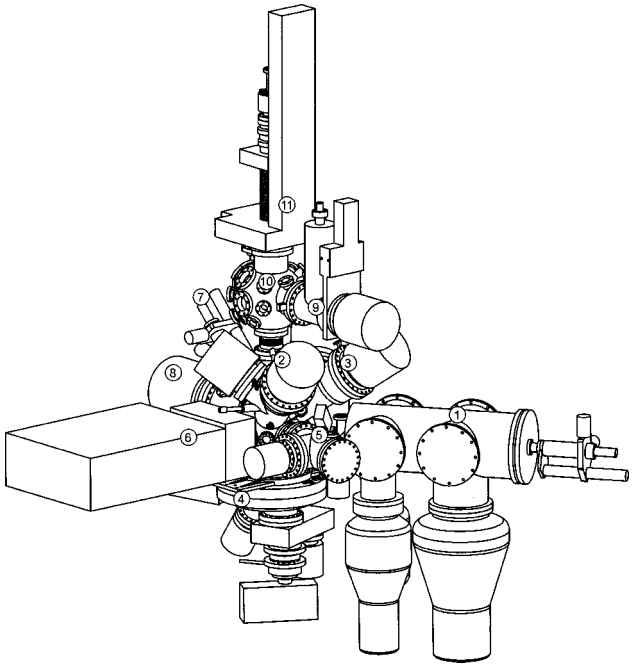

FIG. 2. Overview over the beam system. The labeled components are: (1) beam source 1 (supersonic source), (2) beam source 2 (effusive source), (3) beam source 3 (effusive source), (4) rotatable, differentially pumped detector (QMS 2), (5) stationary detector (QMS 1), (6) FT-IR spectrometer, (7) beam monitor, (8) TMP, (9) Ti sublimation pump/TMP, (10) preparation chamber, (11) manipulator.

(Omicron ErLEED 150) are mounted. High background pressures during preparation are reduced by a gas dosing system, which was previously developed and implemented in other UHV systems.[30] As the preparation of supported catalysts under UHV conditions requires the evaporation of an active component an electron beam evaporator (Omicron EFM3) is required. The evaporator is calibrated using a quartz microbalance (Caburn MDC). Previous studies have shown that a small fraction of ions is produced in the electron beam evaporator source which is then accelerated from the evaporation target (typically on a positive potential of +800 V) toward the grounded sample. The ion bombardment induces defects which may have substantial influence on the growth behavior. During evaporation we therefore apply a bias to the sample, decelerating those ions. A second modification is required due to the fact that area which is covered by the active component is typically larger than the sample area. To avoid evaporation on the sample holder which may lead to artifacts in global reactivity measurements, we have equipped the evaporator with an electrically isolated aperture of exactly the sample size. During evaporation the sample is positioned behind the aperture, which is then also biased via electrical contact to the sample holder.

The test sample is a NiAl(110) single crystal of 11.0 $\times$9.6 mm size and the corresponding preparation procedures are given in Sec. III. The crystal is clamped to a molybdenum sample holder by molybdenum bolts ($M2$). In an attempt to avoid IR radiation from a filament, which may interfere with IRAS measurements, the sample is heated by a 80 W pyrolytic boron nitride/pyrolytic graphite heater (HT-01, Advanced Ceramics) in direct contact with the sample. The temperature is measured by means of a type *K* thermocouple spotwelded to the crystal edge. Finally, the sample holder is attached via a sapphire element to a manipulator, which provides four degrees of freedom. By liquid nitrogen cooling and/or heating sample temperatures between 90 and $>$1300 K can be obtained.

C. Scattering chamber components

After preparation the sample is transferred to the scattering chamber (Pink), which is pumped by a large pumping speed TMP (Pfeiffer TMU1600MC). In comparison to conventional pumps its magnetic suspension reduces vibrations which might interfere with the IR spectroscopy. The scattering chamber has an inner diameter of 300 mm which allows reasonable pumping speeds in the QMS differential pumping stages, and is compatible with a moderate focal length of the IR mirrors of 250 mm (see Sec. II C 6). In the following sections we will describe the setup of the various components (Secs. II C1–II C 6) and their interplay (Sec. II C 7).

1. Supersonic beam source

As the design of supersonic beam sources is well documented in the literature,[24] we will limit ourselves to the basic features of the device. The source consists of an expansion chamber, which is pumped by an unbaffled diffusion pump (Edwards Diffstak 250/2000, 2000 $1\,s^{-1}$, pumping oil Santovac 5) and two differential pumping stages, which are pumped by a liquid-nitrogen baffled diffusion pump (Edwards Diffstak CR160/700, 700 $1\,s^{-1}$, pumping oil Santovac 5) and a TMP (50 $1\,s^{-1}$), respectively. If used in a continuous mode, the supersonic expansion is generated from a 50 μm nozzle (Mo electron microscopy aperture, Plano). Alternatively, a solenoid type pulsed valve with an orifice diameter of 100 μm is used (General Valve Series 9). The pulsed source is driven by a controller which allows a minimum pulse width of approximately 160 μs (General Valve, Iota One). For alignment both nozzles are mounted on a manipulator providing three degrees of freedom. From the expansion a molecular beam is extracted by means of a 0.7 mm skimmer. In the first differential pumping stage the beam can be modulated by a manual beam shutter and a mechanical chopper. The chopper wheel is machined from a 150 mm diam Al disk and is mounted on a home built heavy-duty translation stage operated from the atmospheric side. Depending on its position the beam can be modulated with different duty cycles of 1.5%, 3.3%, or 50%. The chopper wheel is driven by an 400 Hz ac synchronous motor (TRW Globe 75A1008-2) with vacuum compatible lubrication, which is controlled by an ac frequency transformer (REFU 218/02). The motor assembly is clamped into a Cu bronze block with tubes for water cooling, which—under the reduced heat dissipation conditions in vacuum—keep the device at a constant temperature. A synchronization signal is provided by a photodevice. The signal from the photodiode is amplified and discriminated from noise (mainly from the ac motor). Finally, the signal is transformed into 200 μs TTL pulses which can be used as a trigger signal for the multichannel scaler (see Fig. 3). To reduce the pulse width and improve the pulse shape in pulsed valve operation, the rotat-

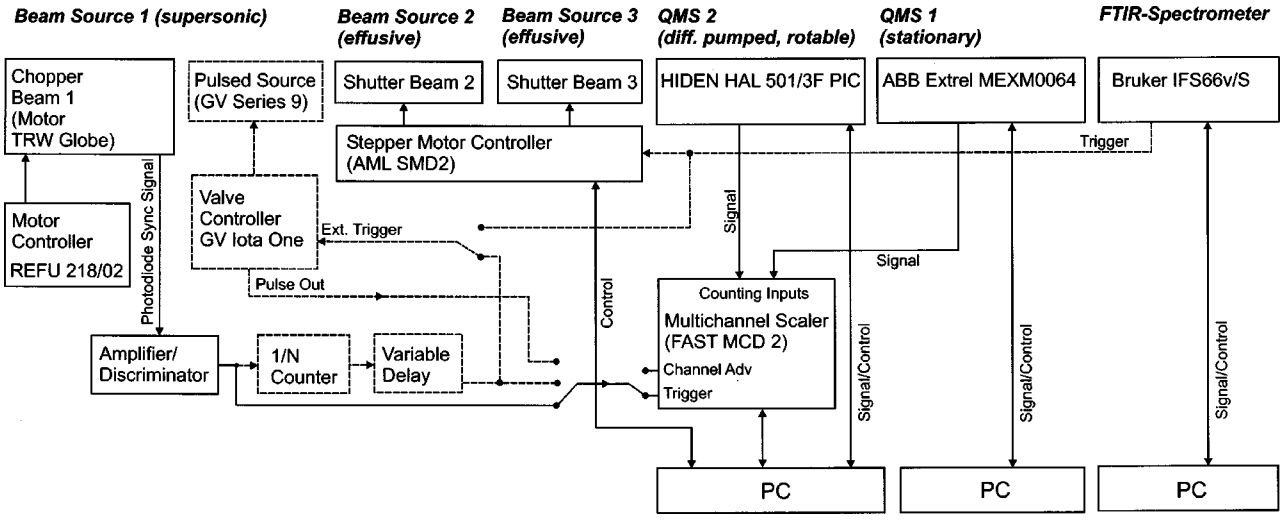

FIG. 3. Schematic data acquisition scheme.

ing wheel chopper can be synchronized with the solenoid valve. This is done by dividing the synchronization signal by an $1/N$ counter to the desired pulsing frequency and externally triggering the valve controller after a delay time which is chosen such that a suitable slice of the pulse is cut out by the chopper wheel.

In the current design the chopper sample distance is 531 mm. Before hitting the sample surface the beam shape is determined by a square aperture. It is located in between the first and the second differential pumping stage to reduce the gas load in the second pumping stage. We can chose from three different square apertures of 2.5, 3.5, and 4.5 mm size on a Cu bronze blade. The aperture is changed from the air side by moving the blade via a linear translator. Due to the incidence angle of 35° the beam profile at the sample is rectangular with an axial ratio of 1.2 and the beam size can be chosen to be smaller or larger than the sample. After passing a second aperture the beam is efficiently separated from the diffuse background gas and enters the scattering chamber. The last aperture has to be large enough not to interfere with the beam at any size. In order to still maintain a low conductance a quadratic aperture of 7.8 mm size was spark cut into a steel cylinder of 40 mm length. In comparison to a flat aperture, the conductance of this tube and thus the effusive load in the main chamber is reduced by a factor of 5.

2. Effusive beam sources

The effusive sources were designed as a tool to expose the sample to a constant and clean gas flux. In comparison to background gas exposure they provide two main advantages: (a) at a given flux they drastically reduce the background pressure and therefore the background signal; and (b) the gas flux can be modulated on a much shorter time scale.

In order to reduce the pumping requirements we have constructed effusive type beams using glass capillary arrays (GCAs) as sources. GCAs have been frequently utilized as gas dosers before.[29] If, however, a homogeneous flux over a larger sample area is required, a device larger than the sample has to be positioned in close proximity to the probe surface. Such requirements are not compatible with angular resolved desorption measurements or a crossing of several beams. We have therefore developed a new design similar to a regular differentially pumped beam source, which allows larger distances from the sample. A cross section of the construction is shown in Fig. 4.

The capillary array (Galileo, 50 μm channel diameter, 1 mm thickness, Fig. 4, No. 15) is located 240 mm from the sample surface. Different types of GCAs have been tested as will be further discussed in Sec. III B. The GCA was sealed with lacquer, cut from a larger piece, and milled to a disk of 12 mm diameter. After processing, the protective sealing was removed and the device was mounted on the source tube sealed by Teflon gaskets (Fig. 4, No. 14). The source tube (Fig. 4, No. 2) is inserted into the inner pumping stage which is pumped by a TMP (Pfeiffer TMU520U, Fig. 4, mounted at flange No. 11) and is connected via a stainless steel hose to the gas inlet flange (Fig. 4, No. 1). The inner pumping stage is mounted on a flexible bellows (VAT, 150 mm i.d., Fig. 4, No. 16) and can be adjusted via two miniature translators

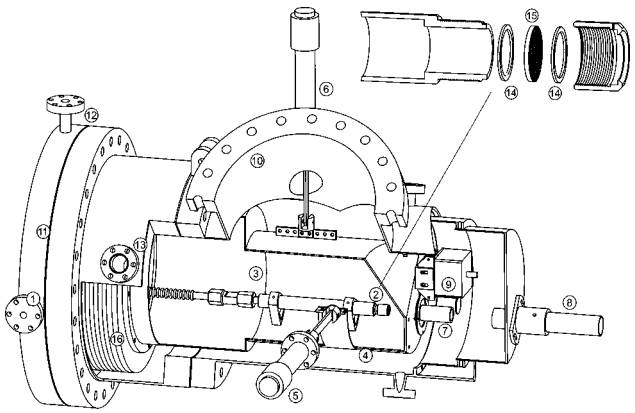

FIG. 4. Effusive beam source. The labeled components are: (1) gas inlet, (2) MCA assembly, (3) inner pumping stage, (4) outer pumping stage, (5) horizontal alignment, (6) vertical alignment, (7) inner aperture tube, (8) outer aperture tube, (9) beam shutter, (10) and (11) flange for TMP, (12) pressure measurement, (13) pressure measurement and electrical connections, (14) Teflon o-ring, (15) MCA.

(Fig. 4, Nos. 5, 6). A UHV stepper motor (AML, B14.1) driven beam shutter (Fig. 4, No. 9) is located in front of the aperture tube (which again minimized the conductance in comparison to a flat aperture, Fig. 4, No. 7), mounted on the front end of the inner pumping stage. It is fully remote controlled and can be used to modulate the beam at arbitrary frequencies up to 10 Hz. In order to maximize the pumping speed and minimize the distance to the exit aperture tube (Fig. 4, No. 8), the outer pumping stage (Fig. 4, No. 4) is constructed as an integral part of the scattering chamber. The second differential stage is pumped by the same type of TMP (Pfeiffer TMU520U, Fig. 4, mounted at flange No. 10). The pressure in both differential stages is controlled by cold cathode gauges (Fig. 4, flanges No. 12, 13).

As the angular orientation of the effusive sources is less critical than that of the supersonic source they are not located in the plane of the angular resolved detector (see Table I). The total angles of incidence with respect to the sample normal are 42.1° for beam 2 and 39.7° for beam 3. Beam source 2 is the exact mirror image of source 3, which is displayed in Fig. 4.

Finally, the required backing pressure for the GCAs of typically 0.01–100 Pa is provided by a two channel pressure control unit which both consist of a upstream flow control valve (MKS 248 A, maximum flow of 10 sccm nitrogen), capacitance manometer (MKS Baratron 122), and pressure controller (MKS Type 250). Before being admitted to the regulation stage the gases are passed through liquid nitrogen cold traps to remove condensable contamination.

3. Beam monitor

The alignment of the three beam sources requires reliable beam intensity and profile measurements. We have therefore set up a simple beam monitor on the principle of an accumulation detector (Fig. 5, No. 2).[31] Its based on a high accuracy ion gauge (Granville-Phillips 360 Stabil-Ion), which is mounted to a 15 mm i.d. stainless steel tube on a CF40 flange. A 16 mm i.d. tube with a 0.1 mm stainless steel membrane parallel to the sample surface is clamped to its front end. A hole in the membrane of 1 mm diameter serves as probe forming an entrance to the detector volume. The assembly is mounted in a miniature manipulator which allows the detector to be positioned exactly at the sample position. It can be utilized for absolute beam intensity and profile measurements independent of the incidence angle and the dynamic properties of the beam. The method is based on a measurement of the pressure variation inside the detector volume, when the beam hits the aperture hole. For nonadsorbing gases (e.g., Ar) the time scale on which an equilibrium pressure p between the beam flux into ($\dot{N}_{\mathrm{in}}=FA$; F: flux density, A:aperture area) and the effusive flux from the detector [$\dot{N}_{\mathrm{out}}=p/(2\pi mkT)^{1/2}$; m, T: mass and temperature of the test gas] is reached depends on the detector volume (180 cm^3) and the aperture diameter (1 mm). This response time can be calculated to be approximately 1.8 s for Ar at 298 K. For gases that can be adsorbed on the detector walls the response times can be significantly longer. After correction for the ionization gauge sensitivity the pressures can be directly converted to absolute beam fluxes. Typically, the background pressure in the detector is about 2×10^{-8} mbar so that the minimum detectable pressure change is 1×10^{-10} mbar. For Ar this corresponds to a flux density of 2.0×10^{10} molecules $\mathrm{cm}^{-2}\,\mathrm{s}^{-1}$.

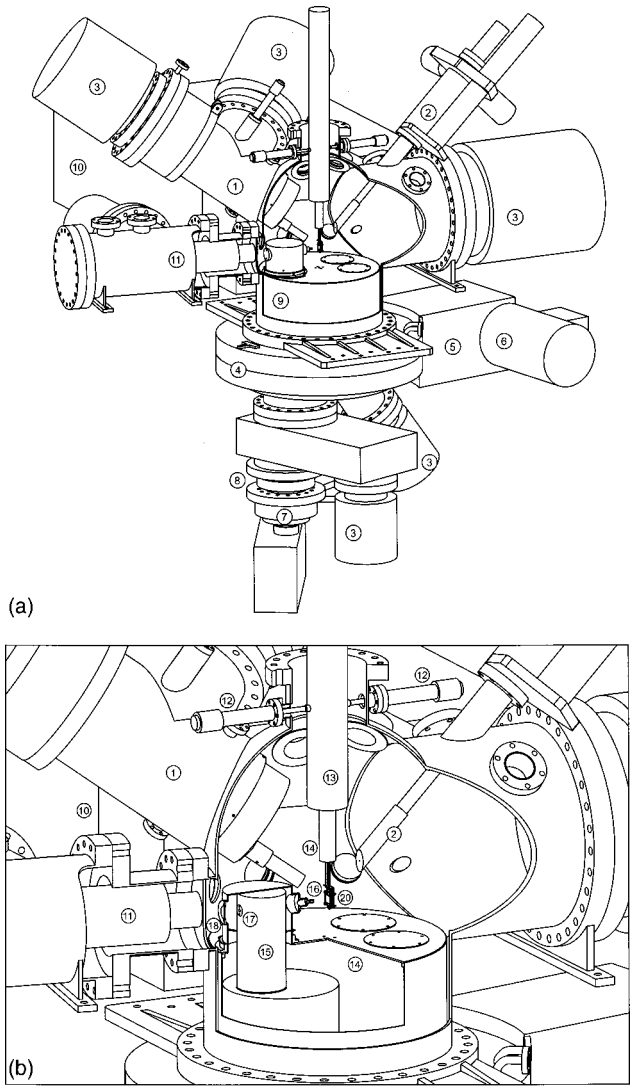

FIG. 5. Scattering chamber overview (a) and closeup (b): (1) beam source 2, (2) beam monitor, (3) TMP, (4) rotatable platform, (5) gear box, (6) ac motor, (7) QMS 2, (8) linear translator, (9) outer pumping stage, (10) FT-IR spectrometer, (11) QMS 1, (12) support tube locks, (13) manipulator support tube, (14) 1-N_2 cryostat, (15) 1-N_2 cooled inner pumping stage, (16) entrance aperture, (17) exit aperture, (18) alignment window, (19) sample holder.

The alignment procedure is such that in a first step the entrance aperture of the beam monitor is set to the focus of the angular resolved detector (see Sec. II C 4). Subsequently, all beam sources are aligned such that the beam profiles are symmetric with respect to the target position. After this the beam monitor is replaced by the sample with its center positioned exactly at the previous beam monitor location. Finally, the IR sample focusing mirrors (Fig. 6, Nos. 8, 11) are aligned with respect to the given sample position (see Sec. II C 6).

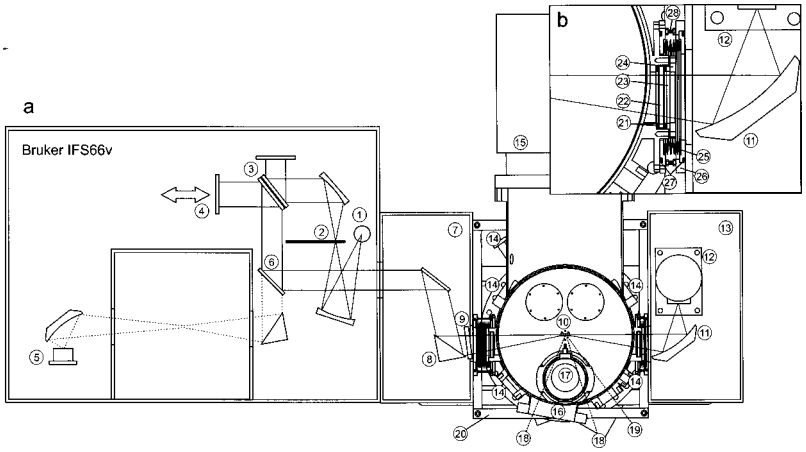

FIG. 6. *In situ* IRAS setup: (1) glowbar, (2) aperture wheel, (3) beam splitter, (4) movable mirror, (5) DTGS detector, (6) movable mirror, (7) mirror chamber, (8) parabolic mirror, (9) MIR polarizer, (10) sample, (11) ellipsoid mirror, (12) MCT detector, (13) detector chamber, (14) alignment windows, (15) TMP, (16) QMS 1, (17) QMS 2, (18) molecular beams 2 and 3, (19) molecular beam 1, (20) support frame, (21) Viton gaskets, (22) KBr window, (23) distance ring, (24) flange ring, (25) bellows, (26) rotatable flange, (27) Viton o-rings, (28) distance locking bolts.

4. Differentially pumped rotatable QMS

The central part of the angular resolved detector [Fig. 5(a), No. 9] is a modified doubly differentially pumped QMS [Hiden HAL 501/3F-PIC, Fig. 5(a), No. 8]. The spectrometer consists of a cross beam ion source (entrance/exit aperture diameter: 4 mm/5 mm), a triple stage mass filter (maximal detectable mass = 150 amu), and a single pulse counting detector. The spectrometer was equipped by Hiden Analytical Ltd. with a first differential pumping stage, the front end which is made of a 60.3 mm o.d. stainless steel tube [Fig. 5(b), No. 15]. In the immediate vicinity of the ionizer it has double walled design and can be cooled by liquid nitrogen. This type of cryoshield can drastically increase the pumping speed for condensable gases.[32] The gas enters the pumping stage through a removable aperture of 2.5 mm diameter (64 mm from the sample surface), crosses the ionizer (located 91 mm from the sample), and exits through an removable aperture of 7 mm diameter (118 mm from the sample). The vertical position of the inner pumping stage can be adjusted by a linear translator [Fig. 5(a), No. 7].

An outer differential pumping stage mounted on a rotary platform completes the detector assembly. Both pumping stages are pumped by TMPs (Pfeiffer TMU260) backed by a turbomolecular-drag/diaphragm pumping stage (Pfeiffer TSU065D). Gas molecules from the sample surface [Fig. 5(b), No. 11] enter this outer stage through an aperture tube [Fig. 5(b), No. 16] of 2 mm i.d. and 10 mm length, the center of which is located 24 mm from the sample. From the current aperture sizes the full angular acceptance of the detector can be estimated to be 6°. During assembly all apertures are aligned such that they focus on a point on the rotation axis of the assembly. This is done via a glass window (Fig. 5, No. 9) behind the exit aperture and with the help of an alignment aid, mounted on the cover of the outer pumping stage cylinder, which marks the later position of the sample center. Also, the window allows later alignment checks. After adjustment, the lateral position of the inner pumping stage with respect to the outer stage is locked with Teflon capped bolts and the detector assembly is mounted to the rotary platform. The ac motor driven rotary platform [Pink, i.d. 300 mm, Fig. 5(a), No. 4] can be operated with a reproducibility better than 0.25°. It is doubly differentially pumped by a rotary pump and a TMP. The pressure rise during operation is below 3×10^{-11} mbar.

5. Stationary QMS

For integral reactivity and sticking coefficient measurements a nondifferentially pumped QMS is required. The spectrometer [ABB Extrel, Fig. 5(b), No. 5] is equipped with an axial ionizer, large quadrupole filter, and a pulse counting multiplier and preamplifier. It is located on the same level as the supersonic beam source and focuses on the sample, so that after integrating an additional differential pumping stage it can also be used for He reflectivity or TOF measurements. For integral reactivity measurements the angular resolved detector is positioned in between the sample and the QMS to block the direct line of sight. Depending on the experiment, data acquisition is accomplished either with the standard controller/software or via a multichannel scaler (see Sec. II C 7).

6. FTIR spectrometer

The vacuum FT-IR spectrometer with time-resolved spectroscopy capabilities (Bruker IFS66v/S) has been modified to meet the special requirements of the beam experiment. The experimental adaptation is schematically shown in Fig. 6. The IR radiation from the SiC glowbar (Fig. 6, No. 1) is focused (mirror focal length $f_1 = 180$ mm) on the aperture wheel (Fig. 6, No. 2). The circular aperture was replaced by an aperture slit ($0.6\,\text{mm}\times4\,\text{mm}$). After passing the interferometer the IR beam exits the spectrometer and enters a separate mirror chamber (Bruker) where it is focused by a parabolic mirror ($f_2 = 250$ mm, Fig. 6, No. 8) onto the sample. The beam size at the sample position can be estimated to be $8\,\text{mm}\times5.5\,\text{mm}$. It is determined by the focal ratio f_2/f_1 and the incidence angle, which was chosen to be 83° with respect to the sample surface (close to the optimum taking into account the finite divergence of the spectrometer optics). As in IRAS on metallic substrates the parallel component of the electric field nearly vanishes close to the surface, and the signal/noise ratio can be improved by selecting only the perpendicular component by a MIR polarizer (Fig. 6, No. 9). The reflected beam is focused by an ellipsoid mirror (Fig. 6,

No. 11, $f_{3,4}=250$, 40 mm) onto the liquid nitrogen cooled mercury–cadmium–telluride (MCT) detector (Bruker).

For several reasons (alignment, magnification) it is advantageous to minimize the focal length of the sample focusing mirrors (Fig. 6, Nos. 8, 11). We have, therefore, built a compact connector to the mirror/detector chamber which is shown in Fig. 6(b): The UHV is separated from the spectrometer vacuum system (~1 mbar) by a KBr window [o.d. 55 mm×5 mm, wedged 0.33° to avoid interference effects, Fig. 6(b), No. 22], sealed by Viton gaskets [o.d. 55 mm, i.d. 45 mm×2 mm, 70 Shore, Fig. 6(b), No. 21]. The spectrometer vacuum flange encloses the UHV flange and acts like a differential pumping stage. It is connected to the detector/mirror chamber via a flexible bellows element sealed by Viton o-rings which can be attached in the expanded position. Both the spectrometer and the detector chamber are mounted on heavy duty linear translators (Rose+Krieger), which allow quick removal for bakeout and precise reconnection. The relative position of mirror and detector chamber is determined by an alignment frame (Fig. 6, No. 20). The position with respect to the UHV chamber is locked by adjustable bolts in the connector flanges [Fig. 6(b), No. 28].

For beam alignment the procedure is as follows: Before mounting it to the UHV system the spectrometer is prealigned with the help of a dummy mirror at the exact sample position and using the support frame to lock the relative position of the detector and mirror chamber. Subsequently, the spectrometer is fully mounted to the beam apparatus. The sample position is set to the focus of the angular resolved detector. Finally, the sample mirrors (Fig. 6, Nos. 8, 11) are adjusted to maximize the reflected IR intensity. After this first coarse alignment, in later experiments only minor adjustments (<0.1 mm) along the sample normal are needed. After optimizing the sample position, the support tube of the manipulator is locked by two Teflon capped miniature linear translators [Fig. 5(b), No. 10] which very effectively reduces vibration of the manipulator support tube.

7. Data acquisition

Schematically, the components of the experiment, the data acquisition, and synchronization for time-resolved experiments are summarized in Fig. 3. Most of the components have been discussed in the previous sections. For time-resolved gas phase measurements the ion pulse signal from the angular resolved detector is analyzed via a multichannel scaler (FAST MCD 2). The TTL synchronization signal is derived either directly from the amplified chopper signal or from the from the pulsed valve controller (see Secs. III A and III C). For integral measurements with QMS1 normally no synchronization is required. However, if a pulsed or chopped beam is used, background pressure modulations might occur and a synchronization with the beam modulation may be advantageous (see Sec. III D). In these cases the chopper or valve output is used as an external channel advance signal. Depending on the required temporal resolution TR-IRAS measurements can be performed in regular or rapid scan mode or—for higher time resolution—via step-scan techniques. The TTL synchronization output from the spectrometer controller can be utilized to trigger the beam shutters or the pulsed valve (see Sec. III E).

III. SYSTEM TESTS AND PERFORMANCE

In the following sections we will report test measurements for the various types of experiments. As a representative sample for the type of model surfaces which will be investigated with the apparatus we will use an ordered alumina film which can be prepared on a NiAl(110) single crystal surface. The preparation and properties of the film have been described previously.[33,34] For the adsorption and reactivity measurements we prepare palladium particles on the alumina film. Also, the growth and structure of such metal deposits has been the subject of several previous investigations,[7,8,35–37] and we will refer to these results in the discussion of the experimental data. Finally, we will use adsorption of CO and O_2 as well as the CO oxidation as a standard test example, as it is one of the best known adsorption and reaction systems and has been studied by beam methods on both single crystals (see e.g., Refs. 2, 38, 39 and references therein) and supported metal particles.[5,40,41]

A. Supersonic beam source

The supersonic beam source can operate with a continuous or a pulsed nozzle. For continuous nozzle operation TOF spectra for the direct beam without sample can be found in Sec. III C. They are taken by rotating the angular resolved detector directly into the beam. The beam intensity at the sample position with Ar (295 K) expanding from a pressure of 3×10^5 Pa is typically 1.0×10^{15} molecules $cm^{-2}\,s^{-1}$ (effective pressure at the sample position 4×10^{-4} Pa). For short pulse operation it is, however, advantageous to use a pulsed source to decrease the gas load. Corresponding TOF spectra for the pulsed source are displayed in Fig. 7(a). The spectra were taken with Ar as a test gas and a backing pressure of 2×10^5 Pa. At a repetition rate of 10 Hz, the time averaged beam intensity for 200 μs pulses as detected by the beam monitor is 1.3×10^{13} molecules $cm^{-2}\,s^{-1}$, corresponding to a total of 1.3×10^{12} molecules $pulse^{-1}$. With an effective pulse width of 350 μs at the sample position this corresponds to an effective pressure of 1.5×10^{-3} Pa. Whereas up to opening times of approximately 200 μs regular pulse shapes are obtained, at larger duration the pulse shape becomes rather complex and might even show several maxima. This behavior is characteristic for solenoid valves[42,43] and is mainly caused by rebound of the closing mechanism. Additionally, the pulse shape is influenced by the time dependent background gas scattering in the expansion chamber. In order to obtain well-defined pulse shapes the chopper is synchronized with the pulsed valve. An example is shown in Fig. 7(a) where the gas pulse was chopped with an opening time of 37 μs (1.5% duty cycle, 400 Hz). The corresponding pulse width at the detector position (82 μs) is dominated by the velocity spread of the Ar molecules.

Measured horizontal beam profiles along the sample surface for the different aperture sizes are displayed in Fig. 7(b) (the horizontal/vertical beam diameter ratio is 1.22/1 due to

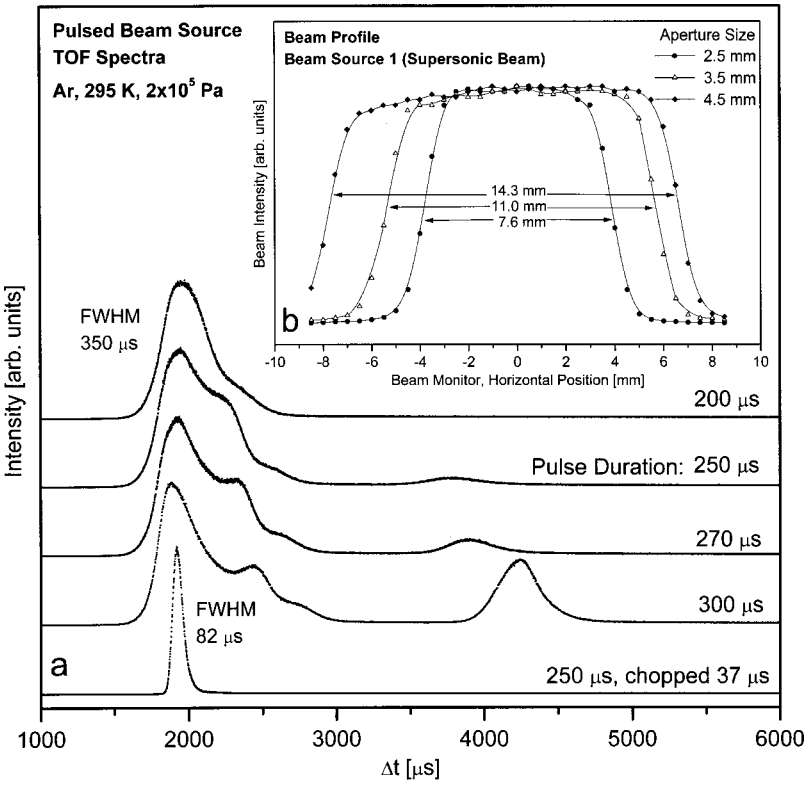

FIG. 7. (a) Solenoid valve pulse shapes for different opening durations. In inset (b) the horizontal beam profile for different aperture sizes is shown.

the incidence angle of 35°). The dimension of the apertures are such that the beam can be chosen to be either smaller (e.g., sticking coefficient measurements) or larger (e.g., IR absorption spectroscopy) than the sample surface (11 mm $\times$9.8 mm). Please note that measured beam profiles represent a convolution of the actual profile with the beam monitor aperture ($\sim$1 mm) which leads to a tailing of the sharp beam edges.

B. Effusive beam sources

The centerline intensity for an Ar beam generated by an effusive beam source is displayed in Fig. 8 as a function of the source pressure. Please note that in contrast to a supersonic beam the intensity of this type of device is gas independent and the beam properties are independent of the source pressure. Both beam sources show a practically identical source pressure intensity behavior. With respect to the beam intensity measurements, no correction for the incidence angle is required, as the beam intensities measured with the beam monitor directly represent the actual flux per unit sample area. We can differentiate between two pressure regimes: At backing pressures below 0.1 mbar we find an exact proportionality to the beam intensity. In the high pressure regime, however, scattering losses result in a decreasing intensity and limit the maximum beam intensity to a value of approximately 2×10^{15} molecules $\mathrm{cm}^{-2}\,\mathrm{s}^{-1}$. In principle

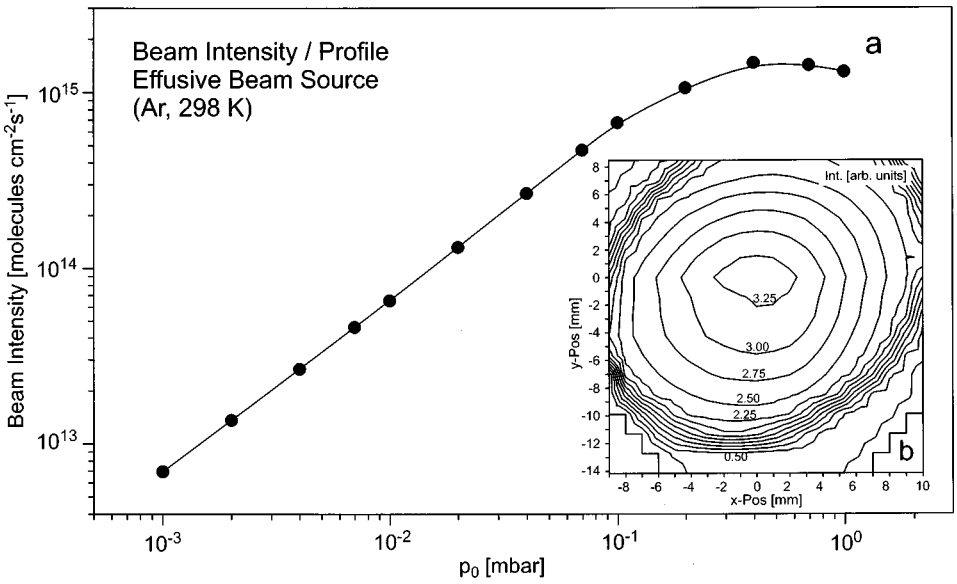

FIG. 8. (a) Effusive source beam intensity as a function of the backing pressure (source 3). The inset (b) shows the beam profile for a backing pressure of 0.1 mbar.

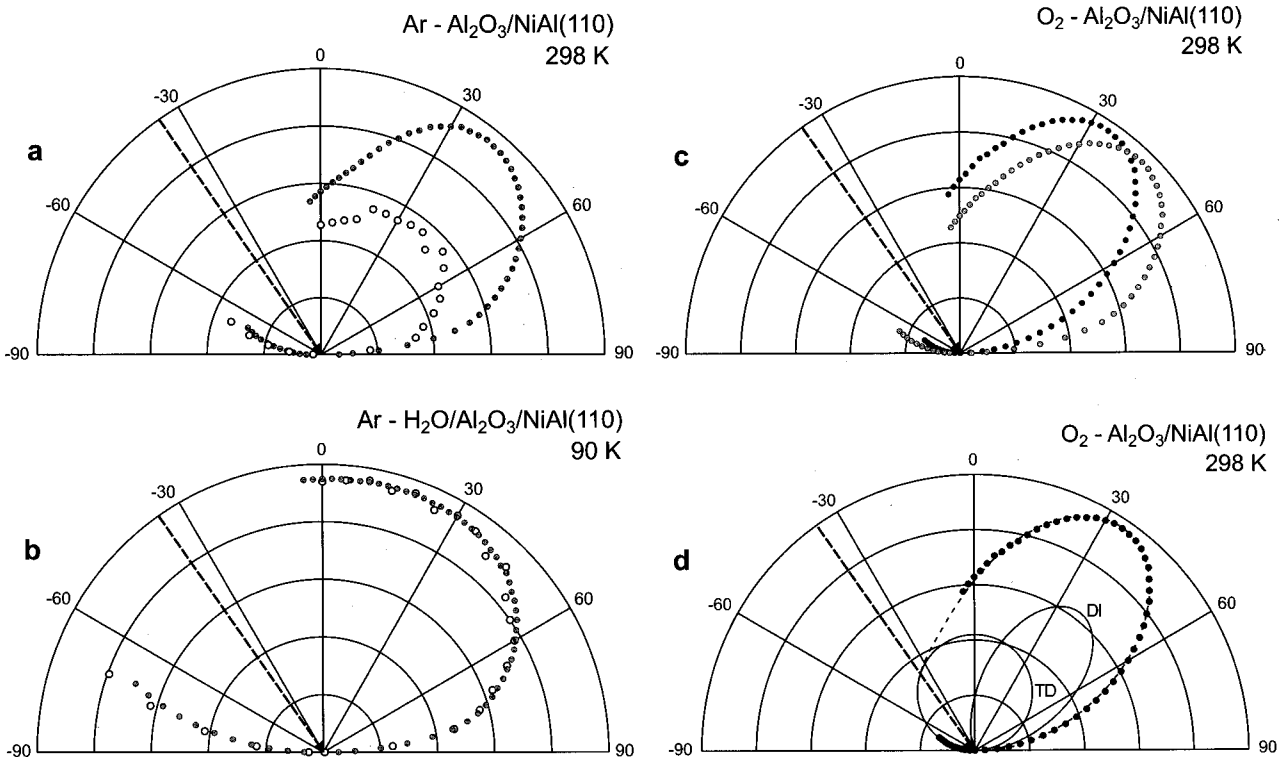

FIG. 9. Angular distributions for scattering of (a) Ar at Al_2O_3/NiAl(110) ($T_{Surface}=298$ K), (b) Ar at an ice multilayer on Al_2O_3/NiAl(110) ($T_{Surface}=90$ K), (c), (d) O_2 at Al_2O_3/NiAl(110) ($T_{Surface}=298$ K). Open symbols: from TOF spectra, gray symbols: from partial pressure, black symbols: normalized to angular acceptance (see the text).

there is no lower limit to the obtainable beam intensities, but in practice, the components of the source pressure regulation system limit the range of controllable values. With the current equipment the lowest obtainable stable beam intensity is approximately 7×10^{12} molecules $cm^{-2}\,s^{-1}$. Lower intensities require a different choice of pressure transducer.

There are two possible reasons for the depletion of the beam at higher intensities. First, there is a contribution due to scattering of the background pressure which will be drastically enhanced as soon as at high pressures the capillary array loses its peaking factor. Additionally, there will be losses due to collisions with other molecules in the beam (due to the velocity and directional spread). Tests with multichannel arrays with smaller channel diameter and larger length/diameter ratio (Hamamatsu, 10 μm channel diameter, 0.5 mm plate thickness) have shown very similar intensity limits, which indicated that the intensity limit is indeed mainly a consequence of intrabeam collisions.

The inset in Fig. 8 represents the two-dimensional beam profile at a source pressure of 0.1 mbar. In the current design the beam diameter was chosen to be larger than the sample to obtain a homogenous exposure during reactivity and IR absorption measurements. The standard deviation from the average beam intensity can be calculated from the beam profile and is approximately 6% over the complete surface of a rectangular sample with given dimensions (11 mm$\times$9.8 mm) and approximately 3.5% over the dimensions of the IR beam (8 mm$\times$6 mm).

C. Differentially pumped rotatable QMS

Angular resolved scattering measurements and TOF spectra for Ar and O_2 interacting with the clean Al_2O_3 film on NiAl(110) and on an ice multilayer grown on the alumina film are shown in Figs. 9 and 10, respectively. The reason for the choice of these systems is that in the case of scattering from the Al_2O_3 film we expect a partial trapping. Although this description is certainly simplified, we can attempt to reduce the scattered gas to a direct inelastic (DI) and a trapping-desorption (TD) component (see e.g., Ref. 3 and references therein). In the case of Ar scattering from ice layers, however, we have a system with complete trapping.[44] On the principle of detailed balance this requires the angular distribution of desorbing Ar to follow a cosine low and the velocity distribution to be angle independent.

We will first discuss the angular resolved data. Please note that for an incidence angle of $+35°$ the range of detection angles between $\theta=-70°$ and $-4°$ is not accessible as here the angular detector shadows the beam. Principally, there are two methods to determine the angular distribution of scattered molecules: (1) the TOF spectra for a pulsed beam are acquired at different scattering angles and are integrated [Figs. 9(a) and 9(b) open circles]; (2) the partial pressure of the scattered gas is detected with a continuous beam as a function of scattering angle [Figs. 9(a) and 9(b), filled circles]. The principal difference between these methods is that in the latter case the signal is dominated by thermalized molecules in the detector, whereas in the former case we discriminate the background and detect only the component directly scattered into the ionizer.

For Ar scattering from the clean alumina film a pronounced asymmetry is found which is due to the DI scattering component. It is evident, however, that the asymmetry is apparently weaker for the time resolved detection method.

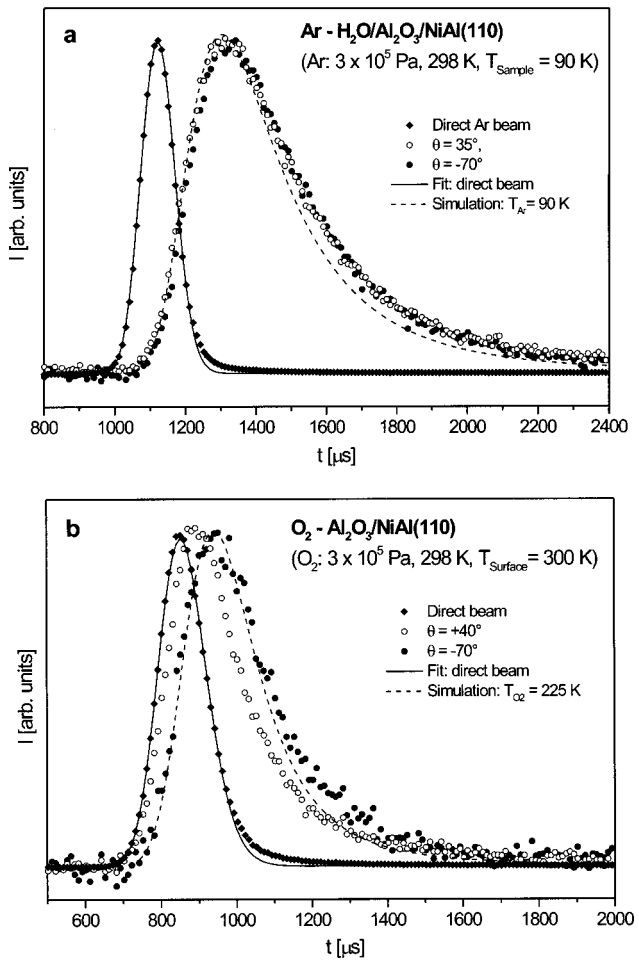

FIG. 10. (a) TOF spectra and fits for Ar scattering at an ice multilayer (on Al_2O_3/NiAl(110)) at $T_{surface}=298$ K and (b) for O_2 scattering at Al_2O_3/NiAl(110) at $T_{surface}=298$ K.

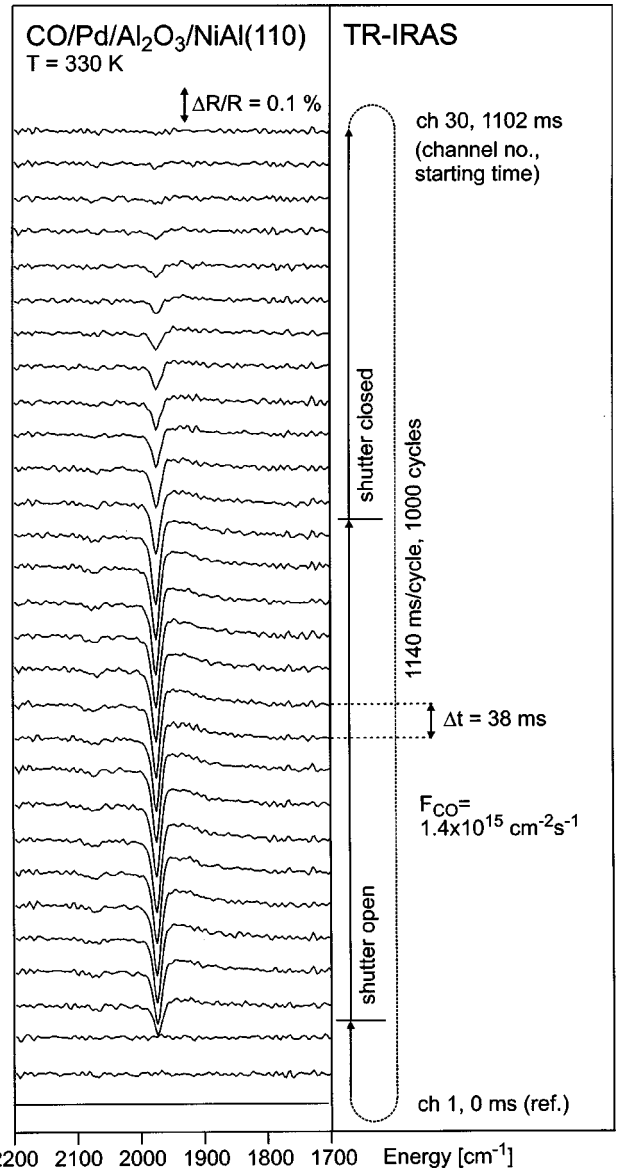

FIG. 11. Time-resolved infrared reflection absorption spectra for a CO/Pd/Al_2O_3/NiAl(110) at $T_{Surface}=330$ K during modulation of the CO flux via beam source 3.

This effect is due to the different velocity distributions of both components. Whereas the DI fraction has a narrow kinetic energy (KE) distribution close to $5/2kT_{Nozzle}$, the TD is characterized by a broad KE distribution centered around lower KE (for complete trapping corresponding to a Maxwell–Boltzmann velocity distribution at $T=T_{Surface}$). As the ionization efficiency is proportional to the flight time in the ionizer and thus inversely proportional to the particle velocity, the detection efficiency for the DI portion is strongly decreased for the time resolved detection method.

In order to obtain angular distributions the signal has to be normalized with respect to the detector acceptance area. For small detection angles θ_{QMS2} the detector is focused such that the detection area is within the beam diameter. For grazing detection angles, however, this is not the case. We have performed angular resolved scattering for Ar on an ice multilayer at 90 K and obtain the experimental angular distribution $I_{exp}(\theta)_{Ar\text{-}ice}$ displayed in Fig. 9(b) (full circles). This system was chosen as it is known to show complete trapping[44] and thus the TD angular distribution must follow the simple cosine law $I(\theta)_{Ar\text{-}ice}\propto\cos(\theta)$. Please note that as a consequence the velocity distribution must be angle independent and of Maxwell–Boltzmann type which is why in this case the time resolved detection mode yields an identical angular distribution [Fig. 9(b), open circles]. In the following $I_{exp}(\theta)_{Ar\text{-}ice}$ was utilized to calibrate the angular distributions as $I(\theta)=\cos(\theta)I_{exp}(\theta)/I_{exp}(\theta)_{Ar\text{-}ice}$.

As an example the angular distribution for O_2 scattered from Al_2O_3/NiAl(110)($T_{Surface}=298$ K) is shown before [$I_{exp}(\theta)_{O_2\text{-}Al_2O_3}$, Fig. 9(c), gray circles] and after calibration [$I(\theta)_{O_2\text{-}Al_2O_3}$, Fig. 9(c), black circles]. As demonstrated in Fig. 9(d), we may finally try to decompose the distribution into a lobular component (DI) and a TD component (possibly including some diffuse scattering from defects). A detailed discussion of the interaction of O_2 and CO with clean and Pd covered Al_2O_3 films will be given elsewhere.[45]

TOF spectra for Ar scattering from an ice multilayer and O_2 scattering from Al_2O_3/NiAl(110) are displayed in Fig. 10. The velocity distribution is determined directly by rotating the angular resolved detector into the beam without the sample in the beam path. Please note the length of the flight path from the chopper to the ionizer (630 mm) is identical for the direct and scattered beam and all delays are due to KE

loss (or sticking) to the sample. To obtain the flight time, the time scale has to be corrected for several contributions such as delays due to the electronics and the QMS and the angle between the chopper photodevice light path and the actual beam path. The latter is determined experimentally by detecting the time delay of the gas pulse as a function of the chopper frequency. In order to obtain the velocity distribution in the direct beam, the TOF spectra were fitted by a MB distribution shifted by a velocity v_0 and characterized by a parallel translation temperature T_0 (see e.g., Refs. 9, and 24). The fits include a convolution with the calculated chopper function [trapezoidal, full width half maximum $=82\,\mu$s for 400 Hz and 3% duty cycle) and correspond to a temperature of $T_0=2$ K at a velocity of $v_0=560\,\mathrm{ms}^{-1}$ for Ar($T_{\mathrm{Nozzle}}=298$ K, 3 bar) and $T_0=9$ K at a velocity of $v_0=720\,\mathrm{ms}^{-1}$ for O_2($T_{\mathrm{Nozzle}}=298$ K, 3 bar).

Please note that in this surface reaction apparatus the sample–ionizer distance was minimized, which precludes good resolution of the final velocity distribution. Still, we will give a brief discussion of some results which illustrate the angular distribution measurements discussed above. Once the velocity distribution of the incoming beam is known, the flux at the sample position can be calculated. The velocity of the scattered species can be determined by convoluting the flux at the sample position with a parametrized velocity distribution for the scattered atoms or molecules and fitting the result to the experiment. A corresponding simulation for a Maxwell–Boltzmann velocity distribution with $T_0=T_{\mathrm{Surface}}=90$ for Ar scattering from an ice multilayer is shown in Fig. 10(a) and compared to the TOF spectra at different detection angles. As expected for the complete trapping case, we obtain a good agreement. Only at the larger detection times we do observe a tailing in the TOF spectra which is probably due to gas accumulation in the detector region. For the partial trapping in the case of O_2 scattering from Al_2O_3/NiAl(110), the TOF spectra depend on the detection angle. Near the specular direction at $\theta=40°$ the TOF spectra contain contributions from both the (fast) lobular DI and the (slow) TD component. At grazing detection angles in backscattering geometry ($\theta=-70°$), the TD component strongly dominates [Fig. 9(d)]. Its velocity distribution is best fitted by a Maxwell distribution with $T_0=0.75\pm0.1T_{\mathrm{Surface}}(225\pm30\,\mathrm{K})$ [Fig. 10(b)].[9]

D. TR-FTIR spectroscopy

In this section we will describe the operation of the of the FTIR spectrometer in time resolved studies, before in Sec. III F we will show how surface (IRAS) and gas phase detection can be correlated in a reactivity experiment.

As a test systems we will employ Pd particles grown on the Al_2O_3/NiAl(110) surface and present some test data for CO adsorption and CO oxidation. A detailed study, in particular addressing the special properties of small Pd particles, will be published elsewhere.[45]

Here, we will focus on only one particular particle size and metal coverage. All systems studied correspond to a Pd coverage of $N_{\mathrm{Pd}}=2.7\times10^{15}\,\mathrm{Pd\,molecules\,cm}^{-2}$, prepared at a deposition temperature of 298 K. With respect to the morphology we can use structural information from previous studies on the growth of Pd particles on the Al_2O_3 film.[7,8,35,36] From scanning tunneling microscopy (STM) and high resolution LEED it is known that the Pd particles form three-dimensional islands which expose preferentially (111) facets. Quantitatively, it was shown that after preparation under these conditions their density will correspond to $0.8(\pm0.1)\times10^{12}$ Pd islands cm^{-2}(STM).[8] Thus there is an average number of approximately 3000 Pd atoms per island and the fraction of the oxide surface which is covered by Pd will be approximately $0.20(\pm0.03)$ (high reolution LEED[7,8]). The fraction of surface Pd atoms will be roughly $0.2(\pm0.04)N_{\mathrm{Pd}}=0.54(\pm0.11)\times10^{15}\,\mathrm{Pdmolecules\,cm}^{-2}$. As large gas exposures at elevated temperature are required, the Pd particles were first stabilized by several oxidation/reduction cycles with O_2 and CO at 366 K. The procedure will be described in detail elsewhere.[45]

Although the temporal resolution capability of FT-IR spectroscopy in the gas or liquid phase is routinely employed up to time resolution in the nanosecond region, examples for TR-IR spectroscopy on surfaces with resolution below 1 s are extremely rare. This is due to the low signal intensity for single reflection IR spectroscopy and the necessity to accumulate data in a surface process which can be driven periodically. Although this is naturally the case in many molecular beam experiments, the variation in surface concentration is in many cases below the detection limit. If we estimate the IRAS detection limit to be 10^{12}–$10^{13}\,\mathrm{molecules\,cm}^{-2}$ and the typical maximal intensities in a beam experiment to 10^{14}–$10^{15}\,\mathrm{molecules\,cm}^{-2}\,\mathrm{s}^{-1}$ we calculate a typical required time resolution in the range of 1–100 ms. In IR spectroscopy this can be achieved by different techniques, such as conventional rapid scan techniques with resolutions down to approximately 10 ms or record-in-flight-techniques[46] or step-scan spectroscopy[47] with time resolution up to 10^{-9} s.

A first example of TR-IRAS on the ms time scale via rapid-scan spectroscopy is presented in Fig. 11. The spectra were acquired for CO adsorption at and desorption from Pd/Al_2O_3/NiAl(110) at a temperature of 330 K. The surface was exposed to CO from the effusive source at a flux of $1.4\times10^{15}\,\mathrm{molecules\,cm}^{-2}\,\mathrm{s}^{-1}$. The beam was modulated at a frequency 0.877 Hz and a duty cycle of 50%. During each modulation period 30 spectra (resolution 8 cm^{-1}) were recorded with an acquisition time of 38 ms/spectrum. 1000 periods were accumulated after an initial stabilizing period of ten periods without data acquisition. The first spectrum was utilized as an internal reference so that the displayed spectra correspond to the change in absorption due to CO adsorption and desorption.

As can be seen in Fig. 11, we can follow the adsorption and desorption kinetics on the time scale of the experiment. Due to the low surface temperature of 330 K the CO coverage during the experiment remains high [on Pd(111) the main desorption temperature in a temperature programmed desorption experiment at a heating rate of 1 $\mathrm{K\,s}^{-1}$ is around

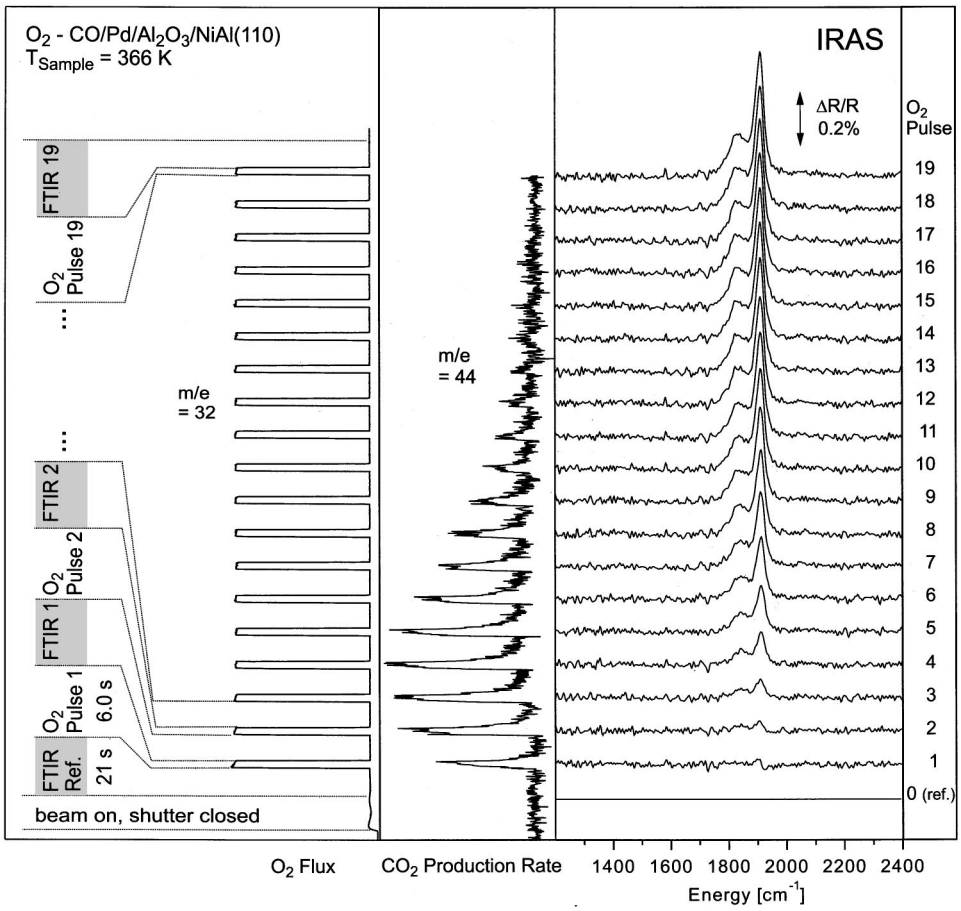

FIG. 12. CO oxidation experiment: O_2 is pulsed on a CO saturated $Pd/Al_2O_3/NiAl(110)$ via beam source 2. The O_2 partial pressure (left), CO_2 production (middle), and IR absorption spectra (right) are measured simultaneously.

460 K.][48] Therefore both the changes in absorption ($\Delta R/R$) due to the compression of the CO layer and the changes in total absorption are detected.

A detailed discussion of the IR spectra of $CO/Pd/Al_2O_3/NiAl(110)$ can be found in the literature[37] and they will not be discussed here. Upon opening of the shutter changes all three spectral CO regions are observed: (1) In the hollow site region (1850 cm^{-1}) we observe a weak positive $\Delta R/R$ corresponding to a decreasing population of these sites. (2) In the on-top region a faint negative peak at 2060 cm^{-1} is observed corresponding to small population of terminal sites which are known to bind CO the weakest.[37] (3) Drastic changes in the spectral region of bridging/hollow CO around 1900–2000 cm^{-1} are found. A shift to lower absorption energy and a broadening[37] gives rise to a positive $\Delta R/R$ on the low frequency side (1900–1950 cm^{-1}) and a dominant negative $\Delta R/R$ on the high energy side (1950–2000 cm^{-1}). Note that in spite of the strong changes in absorption due to the positive and negative contributions the total change in the integral absorption is small and corresponds to about 3% of the total integral CO absorption under these conditions. From sticking coefficient measurements we can estimate the total CO coverage on the $Pd/Al_2O_3/NiAl(110)$ to approximately 10^{14} molecules cm^{-2}, which—for comparison—corresponds to only approximately 10% of the maximum CO number density on a Pd(111) single crystal surface. This example illustrates the remarkable sensitivity of the method in this type of experiments.

E. Surface reactivity studies via correlated FTIR and mass spectroscopy

Finally, we would like to present an example, showing how the kinetics of a reaction can be addressed via correlated gas phase and surface spectroscopy (Fig. 12). As a test reaction we have chosen the CO oxidation as one of the best known surface-catalyzed reactions (Refs. 2, 5, 38–41 and references therein). A detailed study of the CO oxidation on this system will be presented elsewhere.[45]

Similar to the experiments described in the last paragraph we start from a $Pd/Al_2O_3/NiAl(110)$ system, which has been stabilized by repeated O_2 and CO treatment. The surface is then saturated with CO at 366 K. Subsequently an automated experiment is performed in which first a FTIR reference spectrum is acquired (resolution 8 cm^{-1}, acquisition time 21 s). Then O_2 is pulsed via beam source 3 (6 s, 6.5×10^{13} molecules cm^{-2} s^{-1}). After each pulse an IR spectrum is recorded. Simultaneously, the integral CO_2 production rate (in Fig. 12 corrected for the CO_2 response to the O_2 pulse from an blind experiment) and the O_2 background pressure is recorded with QMS 1.

As a detailed analysis of the reaction kinetics is beyond the scope of this article, we will only qualitatively point out which type of information is available from this experiment: (1) Every CO_2 response pulse shows a rise and decay time slower than the originating O_2 pulse being rectangular on the time scale of the experiment. This is due to the limited rate of the surface reaction, the kinetics of which can be extracted

from the wave form.[1,2] (2) The envelope of the wave form represents the overall CO_2 reactive sticking coefficient of O_2 as a function of CO coverage. Due to inhibition of O_2 sticking by CO we find a rising reactive sticking coefficient at high CO coverage, before CO depletion and O_2 coadsorption leads to a decaying probability for CO_2 production. (3) From the simultaneously acquired IR spectra information on the occupation of different sites for the consumed CO is available. Additionally, quantitative information on the surface coverage can be obtained via a coverage–absorption calibration, which can be easily performed by a simultaneous sticking coefficient/IR absorption measurement. Thus, the IR spectroscopy may serve as both a qualitative and quantitative technique, which allows us to efficiently determine the type and coverage of surface species in a single measurement, simultaneously with the gas phase detection described above.

ACKNOWLEDGMENTS

This project has been funded by the Max-Planck-Society and the Deutsche Forschungsgemeinschaft. The authors thank Professor Dr. G. Scoles for his interest and many useful discussions in the initial stage of the project. They are particularly grateful to O. Frank whose work related to solution of numerous technical difficulties was extremely valuable. They would also like to thank the service groups for mechanics and electronics at the FHI which have been substantially involved in the realization of this project.

[1] M. Asscher and G. A. Somorjai, in *Atomic and Molecular Beam Methods*, edited by G. Scoles (Oxford University Press, Oxford, 1988), Vol. 2, p. 489.
[2] M. P. D. Evelyn and R. J. Madix, Surf. Sci. Rep. **3**, 413 (1984).
[3] C. T. Rettner, D. J. Auerbach, J. C. Tully, and A. W. Kleyn, J. Phys. Chem. **100**, 13021 (1996).
[4] P. L. J. Gunter, J. W. Niemantsverdriet, F. H. Ribeiro, and G. A. Somorjai, Catal. Rev. Sci. Eng. **39**, 77 (1997).
[5] C. R. Henry, Surf. Sci. Rep. **31**, 121 (1998).
[6] D. R. Rainer and D. W. Goodman, J. Mol. Catal. A: Chem. **131**, 259 (1998).
[7] M. Bäumer, J. Libuda, and H.-J. Freund, in *Chemisorption and Reactivity on Supported Clusters and Thin Films*, edited by M. Lambert and G. Pacchioni, NATO-Advanced Study Institute, NATO ASI Series E (Kluwer Academic, New York, 1997), p. 61.
[8] M. Bäumer and H.-J. Freund, Prog. Surf. Sci. **61**, 127 (1999).
[9] J. A. Barker and D. J. Auerbach, Surf. Sci. Rep. **4**, 1 (1985).
[10] G. Comsa and R. David, Surf. Sci. Rep. **5**, 145 (1985).
[11] S. T. Ceyer, W. J. Siekhaus, and G. A. Somorjai, J. Vac. Sci. Technol. **19**, 726 (1981).
[12] C. Duriez, C. R. Henry, and C. Chapon, Surf. Sci. **253**, 190 (1991).
[13] L. A. DeLouise, J. Chem. Phys. **94**, 1528 (1991).
[14] M. Rocca, U. Valbusa, A. Gussoni, G. Maloberti, and L. Racca, Rev. Sci. Instrum. **62**, 2172 (1991).
[15] P. M. Holmblad, J. Wambach, and I. Chorkendorff, J. Chem. Phys. **102**, 1 (1995).
[16] M. Bowker, P. D. A. Pudney, and C. J. Barnes, J. Vac. Sci. Technol. A **8**, 816 (1990).
[17] B. N. Eldridge and M. L. Yu, Rev. Sci. Instrum. **58**, 1014 (1987).
[18] M. Balooch, W. J. Siekhaus, and D. R. Olander, J. Phys. Chem. **88**, 3521 (1984).
[19] M. E. M. Spruit, E. W. Kuipers, M. G. Tenner, J. Kimman, and A. W. Kleyn, J. Vac. Sci. Technol. A **5**, 496 (1987).
[20] F. Pradere *et al.*, Rev. Sci. Instrum. **65**, 161 (1994).
[21] M. G. Tenner, E. W. Kuipers, W. Y. Langhout, A. W. Kleyn, G. Nicolasen, and S. Stolte, Surf. Sci. **236**, 151 (1990).
[22] K. D. Gibson and S. J. Sibener, J. Chem. Phys. **88**, 791 (1988).
[23] L. S. Brown and S. J. Sibener, J. Chem. Phys. **89**, 1163 (1988).
[24] *Atomic and Molecular Beam Methods*, edited by G. Scoles (Oxford University Press, Oxford, 1988).
[25] D. F. Padowitz, K. A. Peterlinz, and S. J. Sibener, Langmuir **7**, 2566 (1991).
[26] S. L. Tang, J. D. Beckerle, M. B. Lee, and S. T. Ceyer, J. Chem. Phys. **84**, 6488 (1986).
[27] J. A. Serri, M. J. Cardillo, and G. E. Becker, J. Chem. Phys. **77**, 2175 (1982).
[28] M. Bowker, S. Haq, R. Holroyd, P. M. Parlett, S. Poulston, and N. Richardson, J. Chem. Soc., Faraday Trans. **92**, 4683 (1996).
[29] H. Pauly, in *Atomic and Molecular Beam Methods*, edited by G. Scoles (Oxford University Press, Oxford, 1988), Vol. 1, p. 83.
[30] S. Stempel, Ph.D. thesis, Berlin, 1998.
[31] M. Zen, in *Atomic and Molecular Beam Methods*, edited by G Scoles (Oxford University Press, Oxford, 1988), Vol. 1, p. 254.
[32] P. D. Farrall and T. Engel, Rev. Sci. Instrum. **67**, 4027 (1996).
[33] R. M. Jaeger, H. Kuhlenbeck, H.-J. Freund, M. Wuttig, W. Hoffmann, R. Franchy, and H. Ibach, Surf. Sci. **259**, 235 (1991).
[34] J. Libuda, F. Winkelmann, M. Bäumer, H.-J. Freund, Th. Bertrams, H. Neddermeyer, and K. Müller, Surf. Sci. **318**, 61 (1994).
[35] K. H. Hansen, T. Worren, S. Stempel, E. Laegsgaard, M. Baumer, H.-J. Freund, F. Besenbacher, and I. Stensgaard, Phys. Rev. Lett. **83**, 4120 (1999).
[36] M. Bäumer, J. Libuda, A. Sandell, H.-J. Freund, G. Graw, Th. Bertrams, and H. Neddermeyer, Ber. Bunsenges. Phys. Chem. **99**, 1381 (1995).
[37] K. Wolter, O. Seiferth, H. Kuhlenbeck, M. Bäumer, and H.-J. Freund, Surf. Sci. **399**, 190 (1998).
[38] T. Engel and G. Ertl, J. Chem. Phys. **69**, 1267 (1978).
[39] L. S. Brown and S. J. Sibener, J. Chem. Phys. **89**, 1163 (1988); **90**, 2807 (1989).
[40] C. Becker and C. R. Henry, Surf. Sci. **352**, 457 (1996).
[41] I. Stara, V. Nehasil, and V. Matolin, Surf. Sci. **331**, 173 (1995); **365**, 69 (1996).
[42] M. Izawa, S. Kita, and H. Inouye, J. Appl. Phys. **53**, 4688 (1982).
[43] L. Abad, D. Bermejo, V. J. Herrero, J. Santos, and I. Tanarro, Rev. Sci. Instrum. **66**, 3826 (1995).
[44] P. U. Andersson, M. B. Någård, K. Bolton, M. Svanberg, and J. B. C. Pettersson, J Phys. Chem. A (accepted for publication).
[45] (a) I. Meusel, J. Hoffmann, J. Hartmann, M. Heemeier, M. Bäumer, J. Libuda, and H.-J. Fieund, Catal. Lett. (in press); (b) J. Libuda, I. Meusel, J. Hoffmann, J. Hartmann, L. Piccolo, C. R. Henry, and H.-J. Freund, J. Chem. Phys. (submitted).
[46] (a) G. E. Caledonia, B. D. Green, and R. E. Murphy, J. Chem. Phys. **71**, 4369 (1979); (b) P. M. Aker and J. J. Sloan, *ibid.* **85**, 1412 (1986); (c) T. R. Fletcher and S. R. Leone, *ibid.* **88**, 4720 (1988).
[47] (a) G. V. Hartland, W. Xie, H.-L. Dai, A. Simon, and M. J. Anderson, Rev. Sci. Instrum. **63**, 3261 (1992); (b) L. T. Letendre, H.-L. Dai, I. A. McLaren, and T. J. Johnson, *ibid.* **70**, 18 (1999).
[48] X. Guo and J. T. Yates, Jr., J. Chem. Phys. **90**, 6761 (1989).